Studying the Fluid-Structure Interaction in a Computational Model of the Human Eye During Non Contact Tonometry Tests

Osiris de la Caridad Núñez-Chongo[1(✉)], Claudia Muñoz-Villaescusa[1], Alfo José Batista-Leyva[1], and Francisco Cavas-Martínez[2(✉)]

[1] Higher Institute of Technologies and Applied Sciences, University of Havana, Ave. Salvador Allende 1110, Plaza de La Revolución, 10400 Havana, Cuba
osirisnunez93@gmail.com, abatista@instec.cu
[2] Technical University of Cartagena, Cartagena, Spain
francisco.cavas@upct.es

Abstract. Non contact tonometry (NCT) is a non invasive technique that measures intraocular pressure (IOP), which is one possible way to evaluate the biomechanical behavior of the cornea in vivo and an alternative to determine corneal material parameters. An accurate and reliable numerical model of the non contact tonometry test is required to further understand the eyes response mechanism in accordance with IOP action and the tonometer's air puff. This work developed a model of the human eye based on the finite element (FE) method, a Computational Fluid Dynamics (CFD) simulation of air jet and a fluid-structure interaction (FSI) model by Two-Way dynamic coupling between both systems. A mesh with optimal element densities and good meshing quality was generated. Then, the stress-free geometry of the eyeball was obtained according to IOP loading. As the airflow was selected as incompressible and turbulent during testing, the Spalart-Allmaras turbulence model was included. During the CFD simulation of the air domain, a mesh was generated, with good meshing quality and an estimated time step of 0.0001 s, which allowed reliable results to be obtained at a lower computational cost during this transient analysis. A FSI model was implemented that reproduces the air jet outflow up to its incidence with the corneal surface. A qualitative correspondence was found of the clinical CorVis ST images and the different instances of cornea deformation during simulation. This FSI model between the air puff and the human eye can be considered a starting point to analyze some biomechanical corneal properties during NCT testing for future research purposes.

Keywords: Ocular biomechanics · CorVis ST · Intraocular pressure · Finite element modeling · Computational Fluid Dynamics · Fluid-structure interaction

1 Introduction

Intraocular pressure is the force exerted by humors against inner eye walls. This pressure has been directly and indirectly related to some ocular diseases, such as retinal detachment, ocular hypertension and glaucomatous optic neuropathy. Glaucoma is manifested

F. Cavas Martínez et al. (Eds.): INGEGRAF 2021, LNME, pp. 217–228, 2022.
https://doi.org/10.1007/978-3-030-92426-3_26

by loss of vision with no other apparent symptoms. It may develop due to optic nerve deterioration as a result of either high IOP or other factors in the presence of normal pressure. IOP assessments are crucial factor to diagnose and treatment of this disease [1].

Tonometry is a technique employed to measure IOP that can be performed by contact or non contact. NCT is a non-invasive technique that uses a rapid air pulse to flatten the cornea. During this test, air puff force determines IOP at the applanation time. Advanced optical instruments, such as CorVis ST and the Ocular Response Analyzer (ORA), capture dynamic cornea changes. Although some biomechanical markers of the cornea have been successfully monitored *in vivo*, the main challenge lies in the difficulty of separating the corneal deformation effects that result from IOP action and the deformation effects caused by mechanical stimuli during examinations. For this reason, the design and implementation of mathematical models to predict and characterize the dynamic response of the eyeball have been considered [2].

Some papers have studied NCT theoretically, numerically and clinically. An analytical description consists of representing a dynamic model of the cornea subjected to air puff and IOP loading as a differential equation of a simple harmonic oscillator [3–5]. During computational simulation, the finite element (FE) method is a widely used tool to analyze eye's biomechanical response and the CFD simulation for the tonometer air puff. Two-dimensional (2D) corneal simulations [6, 7] and three-dimensional (3D) simulations to investigate cornea [8] or the entire eyeball's [9, 10] mechanical response are found in the literature. However, these works have some limitations; e. g., they do not include some internal eye structures, or they do not consider internal humors or they ignore the FSI between the air puff and the ocular structure. Other works indicate the importance of considering the fluid-structure interaction effect, but their geometry is based on porcine eyes, 2D and axial symmetry [11]. A more recent study has focused on quantifying the influence of FSI on corneal behavior predictions for patient-specific 3D eye models. However, its limitation lies in it representing only the external eyeball layer [12].

Despite the advances made in numerical models, the studies we found present major simplifications. However, an advanced model that integrates all the previously seen factors is needed to interpret and take advantage of the results. This work proposes performing a dynamic 3D simulation of an NCT test by means of coupling between a CFD model of the air puff and a biomechanical analysis of the human eye by the FE method. The influence of the fluid-structure interaction between air and mainly the anterior surface of an aspheric cornea was considered to achieve a better approximation to the real visual system.

2 Materials and Methods

This study is based on numerical models of the whole eyeball subjected to both IOP and a tonometer air-puff velocity field obtained by CorVis ST. Three important pillars are developed to evaluate the different numerical simulation strategies of a NCT test:

– Human eye numerical model using the FE method.

– A transient and turbulent CFD model that reproduces the air jet during the NCT test.
– Coupling of the fluid-structure interaction between both models.

In order to achieve a correct problem formulation, a series of simulation steps is followed and implemented by the ANSYS Multi-field packages. This program contains the numerical methods and algorithms needed for calculating the separate domains and, finally, for the fluid-structure interaction.

2.1 Human Eye Model Description

A simplified model of the complete human eye was constructed (Fig. 1). The model comprised tissues, such as cornea, limbus, sclera and adipose tissue. This allowed a comparison to be made with similar numerical simulations found in the literature. The geometric parameters of structures were the mean values obtained from the literature. The cornea was considered to be two aspheric surfaces with revolution symmetry around the central axis [13]. The other tissues were described as spherical surfaces of revolution [14].

In addition, boundary conditions were established, and their location, nature and value were fixed. The normal pressure that simulated the IOP caused by aqueous and vitreous humor on inner surfaces was applied to the inner wall. The IOP value was assumed to be 2 kPa (15 mmHg) [13]. A fixed boundary condition (no displacement) was used to limit eye movement on adipose tissue walls. This was where the bony contact and the contact with the six extraocular muscles had to be located [14]. An interface region between the air fluid and anterior eye surface structures was defined.

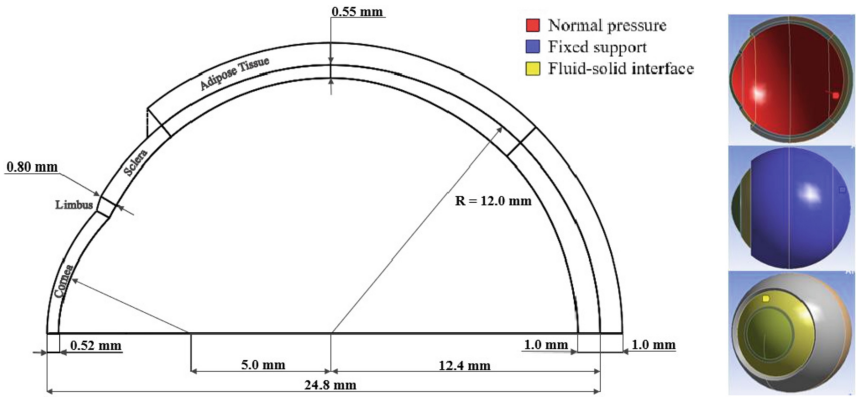

Fig. 1. Lateral view of the simplified eyeball model and the boundary conditions.

Biomechanics behavior was modeled by linear and non linear elastic materials. The material models and parameters for each eye model structure are found in Table 1. Cornea, limbus and sclera were represented by a hyperelastic and isotropic Mooney Rivlin five parameters model [14].

Table 1. Material parameters for the eye model.

Structure	Material Model	Young's modulus	Poisson's ratio	Density	Ref.
Cornea	Hyperelastic	–	–	1400 kg/m^3	[13]
Limbus	Hyperelastic	–	–	1400 kg/m^3	
Sclerotic	Hyperelastic	–	–	1400 kg/m^3	[15]
Adipose Tissue	Isotropic elastic	0.047 MPa	0.47	999 kg/m^3	[16]

To this end, stress-strain curves of cornea [17] and sclera [15] were extracted from the experimental data in the literature to determine the five parameters by the Mooney Rivlin equation [18]. These five parameter were obtained fitting stress-strain curves using ANSYS software, and are shown in Table 2.

Table 2. Parameters of the Mooney Rivlin hyperelastic model obtained in the ANSYS software.

Structure	$C_{10}(Pa)$	$C_{01}(Pa)$	$C_{20}(Pa)$	$C_{11}(Pa)$	$C_{02}(Pa)$
Cornea	3.15117E + 05	3.44546E + 05	1.50620E + 08	2.92175E + 08	1.42642E + 08
Anterior Sclerotic	5,10142E + 07	4,77710E + 07	4,62119E + 10	9,39490E + 10	4,79293E + 10
Equator Sclerotic	2,63660E + 07	2,45856E + 07	9,09079E + 10	1,86423E + 11	9,57846E + 10
Posterior Sclerotic	2,86205E + 07	2,67382E + 07	8,47567E + 10	1,73692E + 11	8,91934E + 10

The technique followed to determine a structure's dynamic response according to the action of any type of time-varying loads was a transient dynamic analysis. This analysis type has been used in ANSYS to establish time-dependent displacements, strains, stresses and forces in a structure [18].

2.2 Air Puff Model Description

A CFD model of the tonometer air puff was represented in a 3D symmetry domain. The domain boundaries were characterized by (Fig. 2): inlet orifice, wall condition, outlet condition (gauge pressure value was zero) and the projection of the anterior surface of the eye. The inlet nozzle was assumed to be aligned with the principal axis of the eye. Symmetry of revolution was considered to simplify the model. The air puff from the inlet orifice lasted 30 ms [12]. The value and direction of the velocity at the entrance to the domain were established by this boundary condition. In Fig. 2, the chart shows the function characterizing the amplitudes of velocities per time by varying the air puff on the nozzle plane, which was obtained from the experimental data fit of the CorVis ST device [12].

The interior domain was occupied by air. The material properties of air are defined in terms of its density (1.204 kg/m^3) and dynamic viscosity (1.83 10^{-5} kg/m·s^{-1}) [12]. Non

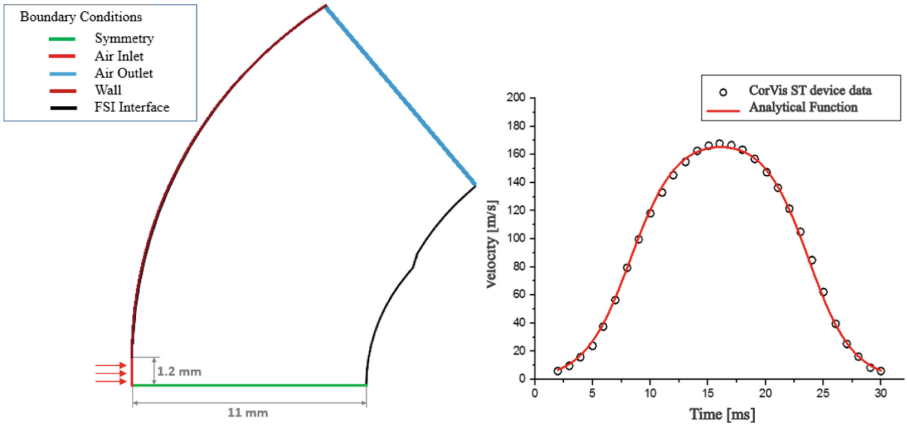

Fig. 2. Boundary conditions for the air jet domain and time velocity profile at the inlet nozzle.

dimensional numbers such as Mach and Reynolds numbers were calculated to define fluid compressibility and motion, respectively. As the Mach number was 0.48, air puff was taken as an incompressible flow. The obtained value of Reynolds number was 23647.05, which meant that a highly disturbed flow with eddies and turbulent vorticities had to be simulated. The Spalart-Allmaras turbulence model has been used in the literature to describe the turbulence of the air flowing out of a tonometer [12].

2.3 Spatial Discretization and Temporal Analysis of the Models

The spatial discretization of both domains was classified as a structured mesh composed of first order prismatic elements. In the air domain, the mesh was generated by a pyramid element with a triangular base and six nodes in a Eulerian configuration (Fig. 3a). A refined mesh was created in the area adjacent to the interface between the fluid and the eye because this is a region of much interest in accuracy terms (Fig. 3b).

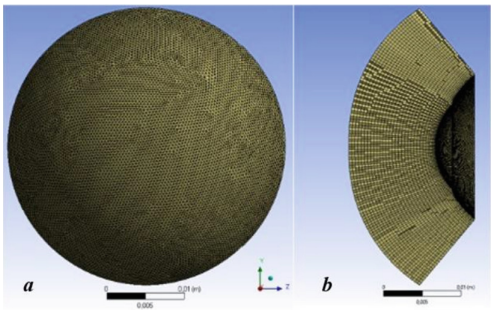

Fig. 3. Spatial discretization in numerical models: air domain mesh.

Eye domain elements were formulated as hexahedral-shaped solid volumes based on a Lagrangian configuration (Fig. 4a, b). Meshing quality was evaluated with the Aspect Ratio, and the Skewness and Orthogonal Quality Metrics. This value was compared to the optimal criteria, as indicated in ANSYS Help [18].

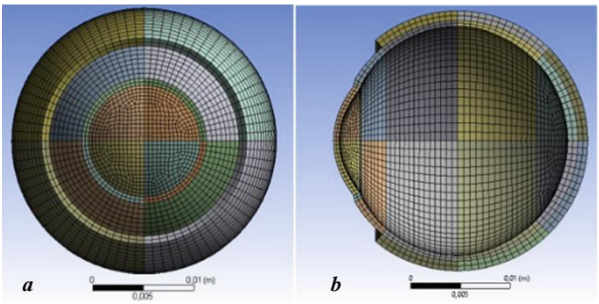

Fig. 4. Spatial discretization in numerical models in the eye domain. a) front view, b) lateral view.

The algorithm employed to obtain the tension-free configuration was applied to the eyeball surface [19]. It was necessary to define the optimal time step size (Δt) for the selected spatial discretization in the air domain. Several transient studies were calculated gradually by decreasing the time step size to reach a balance between the accuracy of the results and the computational cost. The residuals, the number of internal iterations needed for convergence and the Courant Friedrichs-Lewy (CFL) number were monitored during this process [20].

2.4 Fluid-Structure Interaction Models

A dynamic model of the fluid-structure interaction between eye structures and the air puff was constructed and divided into three simulation moments (Fig. 5). First, a stationary analysis (up to 20 ms) was conducted to increase IOP to 2 kPa (black line). In the process a transfer of displacements and forces occurs between the eye domain and the filling air. Secund, a transient analysis (from 20 ms to 30 ms of the simulation) was modeled to stabilize the motion in both domains and IOP is kept constant. Finally, a transient analysis (from 30 ms to 60 ms of the simulation) was done to represent of the NCT air jet. The red line in the graph represents the velocity profile established at the inlet nozzle.

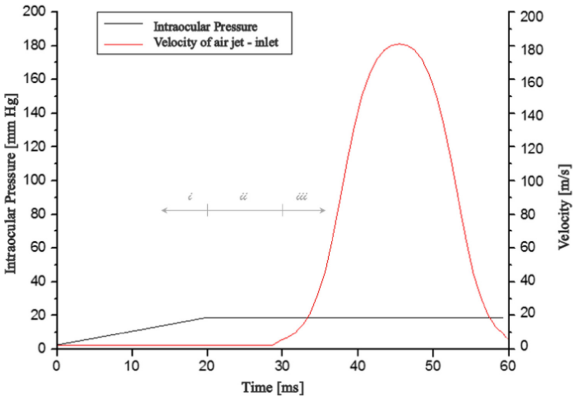

Fig. 5. The numerical simulation FSI moments of the NCT test.

3 Results and Discussion

Modern clinical methods followed to determine IOP and to assess the biomechanical properties of the cornea *in vivo* are based on corneal deformation studies by the air puff effect. A numerical simulation was herein performed by a dynamic analysis to reproduce an NCT test.

3.1 Sensibility Mesh and Free–Stress Geometry Results

The FE method based on mass, force and rigidity matrices was solved to calculate material structure deformations. The mesh density effect on the eye domain's convergence and accuracy was studied across 35 configurations. During the analysis, the size of the generated mesh elements is gradually and uniformly changed. The size of these elements was changed by the surface area (base faces of the prismatic elements in Fig. 4. *a*) in 29 different configurations, and also by the direction of the longitudinal eye slice (lateral edges of the elements in Fig. 4. *b*) in six different configurations, which allowed performing a sensitivity analysis of the mesh per structure. The change in cornea was controlled by varying the number of divisions on edges and meridians to ensure the same length. This was true for the limbus and sclera, but not for the adipose tissue elements, which acted as subordinate elements.

Variation in apical displacement, Von-Mises stress and maximum principal stress due to the IOP action were studied in the different configurations. The radial expansion at the scleral equator was also measured [9].

Table 3 shows the meshing arrangement obtained for each eye structure. The results showed that for a mesh size of approximately 43607 nodes, the changes in apical displacement and radial expansion at the sclera equator were less than 0.05%, and were below 2.0% for the maximum principal stress and Von-Mises stress. This allows us to select the mesh with the values shown in Table 3.

Table 3. Mesh composition for each eye structure.

Eye structure	Cornea	Sclera	Limbus	Adipose Tissue	Total
Number of elements	3888	9288	1080	14328	36144
Number of nodes	5760	24148	1920	20308	43607

The effect of mesh density on the accuracy of the strain values and computational cost can also be observed by analyzing the displacement field. Figure 6 compares the displacements obtained by an increase in IOP up to 2 kPa (15 mmHg) for different mesh densities. The results showed a significant difference in the displacements between the mesh of 2038 elements and that of 36144 elements, which was not the case when the number of elements was increased up to 143625.

In the coarse mesh, cornea apical displacement was 0.2574 mm, which did not coincide with the maximum anterior cornea surface displacement in relation to the X-axis direction (0.2617 mm). However, the results were similar when comparing the optimal mesh (configuration of Table 3) and a much more refined mesh. The maximum displacements coincided with the apical displacements on the cornea with values of 0.2820 mm and 0.2837 mm for each mesh, respectively. The displacement values in the normal direction to the surface were 0.002848 mm, 0.002730 mm and 0.002712 mm for each mesh, respectively. Also the displacement values in the normal direction to the surface were 0.002848 mm, 0.002730 mm and 0.002712 mm for each mesh when refining respectively. The results showed minor differences between magnitudes for the last two mesh configurations (~20 nm). The results obtained with the most refined mesh were 23-fold slower than the mesh selected as the optimal one. After this analysis, the mesh of 36144 elements achieved an adequate balance among the minimum configuration of the number of elements, accuracy and computational time.

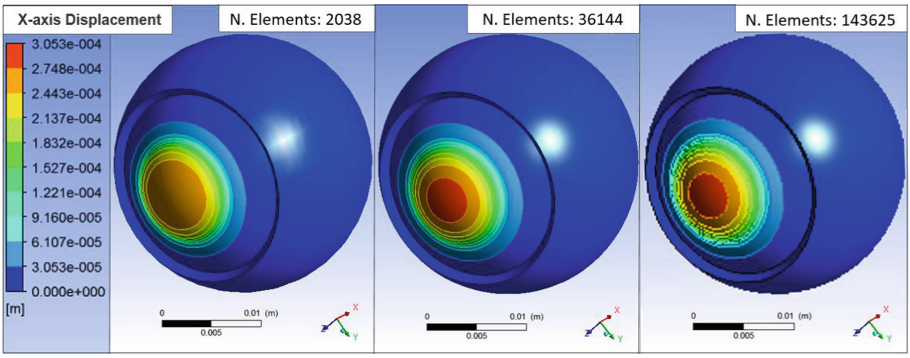

Fig. 6. Displacement field contours of the eye model for different mesh densities, the number of elements for each configuration are shown.

The mesh quality results were adequate. The maximum aspect ratio metric value was 3.4, but its values were distributed with a mean value of 2.04, agreeing with the optimal

metric criterion of the elements. The skewness results showed that more than 80% of the elements had excellent metrics according to the criterion. The orthogonal quality of elements came close to 1 and the minimum reported value was 0.49, a criterion that indicates a good mesh [18].

The displacement-based algorithm employed to obtain a stress-free configuration was applied to the anterior and posterior corneal surfaces, the limbus surfaces and the sclera surfaces. In these geometries, an estimated maximum error of 0.005 mm was found in the third iteration of the algorithm, which was lower than the tolerance chosen to finalize the process. The new geometric parameters of the aspheric cornea surfaces were found for the model. However, the changes in the geometric parameters of the sclera surfaces were not significant compared to the values obtained for the cornea. This result can be explained by the greater sclera stiffness.

A CFD model of the air puff governed by momentum, continuity and turbulence equations was developed to calculate the pressure and velocity fields of flow. Several transient calculations for Reynolds-averaged Navier-Stokes equations (RANS) were conducted. The difference from one complete calculation to the other was based on the gradual decrease of the time step size (Δt). The analysis evidenced that the maximum number of iterations required for convergence of equations decreased approximately with a lowering Δt. In addition, the maximum CFL at the flow-sensitive locations decreased and computational time increased as Δt lowered. The results showed that for a time step size of 0.0001 s, a balance between the accuracy of the results and the computational cost was achieved. This result can guarantee the stability and efficiency of the convergence process of the solutions over the transient region of the air-fluid domain.

3.2 Qualitative Analysis of the Fluid-Structure Interaction Model

To be able to account for the interaction effect of air on the eye structure's response to loading, the two domains had to be solved simultaneously in a *Two-Way* coupling, which allowed data to be interchanged in each time step of the solution. Finally, a dynamic model of the fluid-structure interaction between eye structures and air puff was constructed. During the FSI numerical simulation, the main corneal states while testing were identified. Figure 7 shows two of these states: the first applanation (*a*) at about 39 ms and the maximum concavity (*b*) at roughly 46.1 ms.

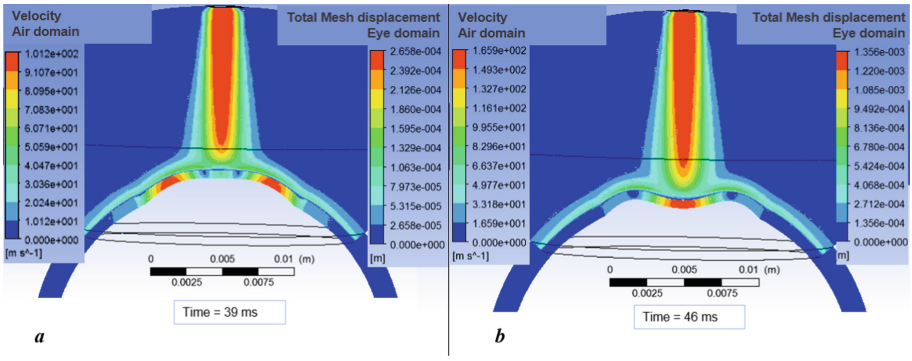

Fig. 7. The FSI model at the first applanation moment and upon maximum concavity.

The NCT test was successfully represented by making a qualitative comparison to the corneal deformations acquired during the clinical Corvis ST tests for human eyes *in vivo*. In Fig. 8, clinical images are observed at six time points of the FSI numerical simulation. The results showed a good agreement of corneal deformations, but they were not perfectly equal. This could be due to differences in geometry, IOP and material properties. Consequently, tests done with real patients differ from the average values assumed in the model. Some studies have also shown that the same displacements can be obtained for different combinations of these parameters [9].

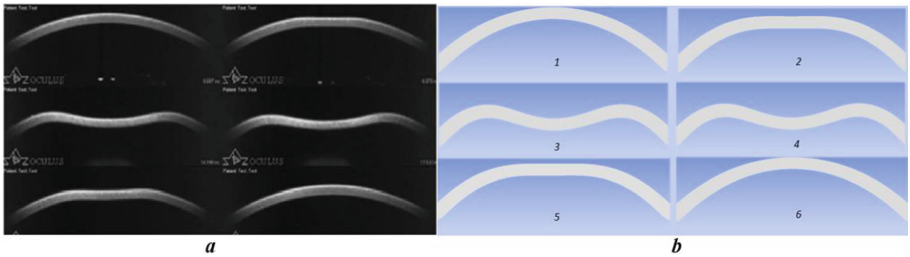

Fig. 8. The CorVis ST images [2] recorded during NCT testing (*a*) and the numerical corneal configuration (*b*). Time of comparison: 1) Physiological configuration, 2) First applanation, 3) Configuration at maximum air jet pressure, 4) Configuration at maximum apex displacement, 5) Second applanation, 6) New physiological configuration after testing.

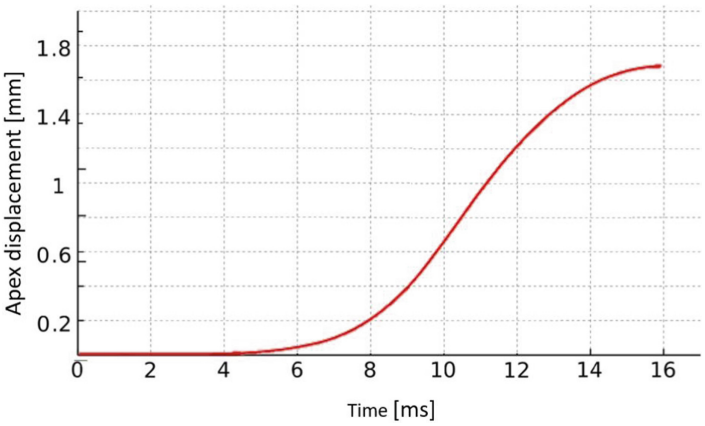

Fig. 9. Time evolution of the maximum corneal apex displacement for the simulations conduced.

The apex displacement of the cornea was analyzed during half of simulation time history conducted (Fig. 9). The displacements obtained for the modeling of the fluid-structure interaction model were within the ranges reported in the numerical models in the literature [9]. In some numerical models presented in the literature, the corneal apex deformation may have diverse responses during a numerical simulation of the air puff

experiment. *Ariza et al.* [9] demonstrated that the same apical displacement can occur for different combinations of corneal material properties and IOP values. Then, an exact numerical value may vary depending on the properties and parameters assumed for each numerical model.

4 Conclusions

A numerical simulation was developed to reproduce an NCT test and to represent some of the dynamic response parameters of the human eye in accordance with IOP action and the tonometer air puff. The FSI between the human eye and air puff fluid was considered in the numerical model. For this purpose, an FE model of the human eye with internal structures and a CFD model of air fluid were developed.

The main results were: a model of the eyeball using FE analysis with optimal spatial discretization and a good mesh quality for the chosen eye geometries and material properties. The stress-free geometry of the eyeball affected by IOP action was obtained.

The CFD model was implemented by a transient analysis that reproduced the air puff outflow until its incidence on the corneal surface. Air fluid was considered to be incompressible and turbulent during testing and was numerically characterized by the Spalart-Allmaras turbulence model. In the air domain, a mesh with both good meshing quality and an estimated time step of 0.0001 s was generated, which gave reliable results at a reasonable computational cost during this transient analysis.

The NCT test was reproduced by a numerical simulation of the fluid-structure interaction by coupling among the above models: the information exchange between the two domains was framed within a dynamic interaction model with strong *Two-Way* coupling.

The six main experimental test states were reproduced by the numerical simulation. A correspondence was noted in the qualitative comparison of the clinical images acquired from Corvis ST and cornea deformation during the numerical simulation. A non contact tonometry test was reproduced by numerical simulation, including a dynamic analysis of the fluid-structure interaction between the test air pulse and the ocular structure model. This FSI model between air puff and the human eye will be taken as a starting point to analyze some biomechanical cornea properties during NCT testing performed for future research purposes.

Acknowledgements. We wish to thank the assistance and cooperation between the Polytechnic University of Cartagena, Spain, and the Higher Institute of Technologies and Applied Sciences, University of Havana, Cuba. This collaboration was funded by the Fundación Carolina with the 2020SEGIB mobility program.

References

1. Conti, F.: Fisiología de la visión, en Fisiología médica, McGraw-Hill, Ed., ed. España, pp. 379–408 (2010)
2. Montanino, A., Angelillo, M., Pandolfi, A.: Modelling with a meshfree approach the cornea-aqueous humor interaction during the air puff test. J. Mech. Behav. Biomed. Mater. **77**, 205–216 (2018)

3. Han, Z., et al.: Air puff induced corneal vibrations: theoretical simulations and clinical observations. Refractive Surger **30**, 208–213 (2014)
4. Simonini, I., Angelillo, M., Pandolfi, A.: Theoretical and numerical analysis of the corneal air puff test. J. Mech. Phys. Solids **93**, 118–134 (2016). https://doi.org/10.1016/j.jmps.2016.04.012
5. Kaneko, M., Tokuda, K., Kawahara, T.: Dynamic sensing of human eye. In: Presented at the Conference of Robotics and Automation, Barcelona, Spain (2005)
6. Kling, S., Bekesi, N., Dorronsoro, C., Pascual, D., Marcos, S.: Corneal viscoelastic properties from finite-element analysis of in vivo air-puff deformation. PLoS ONE **9**(8), e104904 (2014)
7. Roy, A.S., Kurian, M., Matalia, H., Shetty, R.: Air-puff associated quantification of non-linear biomechanical properties of the human cornea in vivo. J. Mech. Behav. Biomed. Mater. **48**, 173–182 (2015)
8. Montanino, A., Angelillo, M., Pandolfi, A.: A 3D fluid-solid interaction model of the air puff test in the human cornea. J. Mech. Behav. Biomed. Mater. **94**, 22–31 (2019). https://doi.org/10.1016/j.jmbbm.2019.02.030
9. Ariza-Gracia, M., Zurita, J.F., Piñero, D.P., Rodriguez-Matas, J.F., Calvo, B.: Coupled biomechanical response of the cornea assessed by non-contact tonometry. A simulation study. PLoS One **10**(3), e0121486 (2015)
10. Muench, S., Roellig, M., Spoerl, E., Balzani, D.: Numerical and Experimental Study of the Spatial Stress Distribution on the Cornea Surface During a Non-Contact Tonometry Examination. Exp. Mech., 59, 1285–1297 (2018)
11. Ariza-Gracia, M., Wu, W., Calvoa, B., Malv, M., Büchlere, P., Rodriguez Matas, J.F.: Fluid-structure simulation of a general non-contact tonometry. A required complexity? Comput. Methods Appl. Mech. Eng. **340**, 202–215 (2018)
12. Maklad, O., Eliasy, A., Chen, K.J., Theofilis, V., Elsheikh, A.: Simulation of air puff tonometry test using arbitrary lagrangian-eulerian (ALE) deforming mesh for corneal material characterisation. Int. J. Environ. Res. Public Health **17**(1), 54 (2019)
13. Muñoz-Villaescusa, C.: Modelo biofísico del ojo humano: Su aplicación en cirugía LA- SEK. Tesis de diploma, Instituto Superior de Tecnologías y Ciencias Aplicadas, La Habana (2014)
14. Núñez-Chongo, O.: Modelación en elementos finitos del ojo humano. Tesis de Diploma, Instituto Superior de Tecnologías y Ciencias Aplicadas, La Habana (2016)
15. Elsheikh, A., Geraghty, B., Alhasso, D., Knappett, J., Campanelli, M., Rama, P.: Regional variation in the biomechanical properties of the human sclera. Exp. Eye Res. **90**(5), 624–633 (2010)
16. Uchio, E., Ohno, S., Kudoh, J., Aoki, K., Kisielewicz, L.T.: Simulation model of an eyeball based on finite element analysis on a supercomputer. Brit. J. Ophthalmol. **83**(10), 1106–1111 (1999)
17. Elsheikh, A., Alhasso, D., Rama, P.: Biomechanical properties of human and porcine corneas. Exp. Eye Res. **86**(5), 783–790 (2008)
18. ANSYS: Mechanical APDL Theory Reference. Release 18.0. ANSYS, Inc. South- pointe, 275 Technology Drive Canonsburg, PA (2018)
19. Elsheikh, A., Whitford, C., Hamarashid, R., Kassem, W., Joda, A., Büchler, P.: Stress free configuration of the human eye. Med. Eng. Phys. **35**, 211–216 (2013)
20. ANSYS: Fluent Theory Guide. Release 15.0: ANSYS, Inc. Southpointe, 275 Technology Drive Canonsburg, PA (2013)